

RESEARCH ARTICLE

10.1002/2016JB013395

Evolution of young oceanic lithosphere and the meaning of seafloor subsidence rate

Tomoko Korenaga¹ and Jun Korenaga¹¹Department of Geology and Geophysics, Yale University, New Haven, Connecticut, USA

Key Points:

- We have constructed a new integrated geophysical and petrological model for the evolution of oceanic lithosphere
- The new model predicts a subsidence rate of $\sim 500 \text{ m Myr}^{-1/2}$ considerably faster than the observed value of $\sim 320 \text{ m Myr}^{-1/2}$
- The observed subsidence rate points to the combined effect of incomplete viscous relaxation and dynamic topography

Correspondence to:

T. Korenaga,
tomoko.korenaga@yale.edu

Citation:

Korenaga, T., and J. Korenaga (2016), Evolution of young oceanic lithosphere and the meaning of seafloor subsidence rate, *J. Geophys. Res. Solid Earth*, 121, 6315–6332, doi:10.1002/2016JB013395.

Received 23 JUL 2016

Accepted 30 AUG 2016

Accepted article online 5 SEP 2016

Published online 21 SEP 2016

Abstract Plate tectonics, a special class of mantle convection so far observed only on the Earth, is responsible for a vast array of geological processes, from the generation of continental crust to the modulation of atmospheric composition. Whereas conditions for its operation are still debated, the minimum requirement is generally thought that surface plates become denser than the underlying asthenosphere so that they can subduct. Recent studies, however, have raised the possibility that even mature oceanic plates remain buoyant because chemical buoyancy is too high to be overcome by negative thermal buoyancy, challenging the basic tenet of plate tectonics. Here we show that on the basis of new integrated geophysical and petrological modeling, oceanic plates do become negatively buoyant after $\sim 30 \text{ Myr}$. Our modeling also indicates that the seafloor would subside at a rate of $\sim 500 \text{ m Myr}^{-1/2}$, which is considerably faster than the observed rate of $\sim 320 \text{ m Myr}^{-1/2}$. We suggest that this discrepancy in subsidence rate is best explained by the combined effect of incomplete viscous relaxation within oceanic plates, radiogenic heat production in the convecting mantle, and the secular cooling of the Earth.

1. Introduction

The convective cooling of the Earth's mantle exhibits itself as the formation of new seafloor at mid-ocean ridges and its subsequent deepening, and a proper understanding of this elementary process of mantle convection is still surprisingly elusive. Hot mantle ascending beneath mid-ocean ridges melts partially to create basaltic oceanic crust, and the crust as well as the residual mantle after melting (called the depleted lithospheric mantle) are compositionally less dense than the mantle before melting (the asthenosphere) [Oxburgh and Parmentier, 1977]. This chemical buoyancy is usually thought to be compensated eventually by negative thermal buoyancy; a cold boundary layer formed by surface cooling, also known as thermal lithosphere, becomes sufficiently thick after a few tens of million years (Myr) [Oxburgh and Parmentier, 1977; Davies, 1992]. Once subducted, buoyant basaltic crust can transform to dense eclogitic crust [Ringwood and Green, 1964], but the achievement of negative buoyancy before subduction is essential for the initiation of subduction. Recent studies, however, have raised the possibility that even mature oceanic plates at present are not negatively buoyant [e.g., Hynes, 2005; Valencia and O'Connell, 2009], and because plate tectonics is nonetheless happening, the initiation of subduction may be controlled by other factors such as external compression [e.g., Gurnis et al., 2004]. Such external forcing depends on the evolving force balance of plate tectonics, so understanding the onset of subduction (and thus the onset of plate tectonics itself) would become a chicken-and-egg problem.

Through thermal contraction and isostatic adjustment, the growth of the cold boundary layer also leads to the deepening seafloor away from mid-ocean ridges [Davis and Lister, 1974; Parsons and Sclater, 1977]. The seafloor subsidence defines the water capacity of ocean basins, with first-order influence on sea level variations [Parsons, 1982]. The observed subsidence rate of $\sim 320 \text{ m Myr}^{-1/2}$ [Korenaga and Korenaga, 2008], however, appears to be too low to be explained by the thermal expansivity of mantle minerals [Korenaga, 2007a; Grose and Afonso, 2013], presenting another challenge for our theoretical understanding of the evolution of suboceanic mantle. Two disparate mechanisms have been put forward to explain this discrepancy: reduction in effective thermal expansivity caused by incomplete viscous relaxation within oceanic lithosphere [Korenaga, 2007a] and dynamic topography caused by radiogenic heat production in the sublithospheric mantle [Korenaga, 2015]. It is currently unresolved which mechanism is more important.

To address these issues on the cooling of suboceanic mantle and its consequences, we have developed a new integrated geophysical and petrological model. In this paper, we model thermal evolution for the duration

of 100 Myr and focus on the first ~70 Myr. Seafloor older than ~70 Myr old is known to deviate from the prediction of simple half-space cooling [Parsons and Sclater, 1977; Stein and Stein, 1992], and such deviation can be explained by, for example, the occurrence of small-scale convection [Huang and Zhong, 2005; Korenaga, 2015]. Here we restrict ourselves to the simple, early phase of lithospheric evolution. As we will demonstrate in this paper, understanding this early phase is not as straightforward as commonly believed, and to properly interpret our modeling results, it is necessary to extend our scope substantially, even to the secular cooling of the Earth. We begin with describing our theoretical formulation.

2. Numerical Modeling of Thermal Evolution

The thermal evolution of the suboceanic mantle is modeled by solving the following one-dimensional equation of heat conduction:

$$\rho(P, T)C_p(P, T)\frac{\partial T}{\partial t} = \frac{\partial}{\partial z} \left(k(P, T)\frac{\partial T}{\partial z} \right), \quad (1)$$

where ρ , C_p , k , P , T , t , and z are density, specific heat, thermal conductivity, pressure, temperature, time, and depth, respectively. The model spans from the seafloor ($z = 0$) to the depth of 300 km, which is sufficiently deep to model half-space cooling for the duration of 100 Myr. The above equation is solved with a finite difference approximation, using the vertical spacing of 1 km and the time step of 5000 years. The initial temperature profile is the adiabat with the potential temperature (referenced at the surface, T_{p0}) of 1623 K (1350°C) [Herzberg *et al.*, 2007], and the surface temperature is fixed at 273 K (0°C).

Some recent studies on the integrated geophysical-petrological modeling of the suboceanic mantle [Afonso *et al.*, 2008; Grose and Afonso, 2013] adopt the concept of the so-called plate model [e.g., McKenzie, 1967; Parsons and Sclater, 1977; Stein and Stein, 1992] and fix the model temperature at a relatively shallow depth (~100 km), which helps to explain the deviation from the prediction of half-space cooling. For the first 70 Myr of thermal evolution, which is of our primary interest, simple half-space cooling has long been considered to be adequate, and we do not impose a temperature boundary condition except for the surface; for the model depth of 300 km and the duration of 100 Myr, the cooling front does not reach the bottom. That is, our model is sufficiently deep to approximate the cooling of a semi-infinite solid. Using the bottom temperature condition as in the plate model could affect not only the evolution after the first 70 Myr (e.g., seafloor flattening) but also the earlier phase (e.g., reduced seafloor subsidence), and for the latter, it is difficult to defend the artificial temperature condition in a physically reasonable manner. If one tries to justify the plate model using small-scale convection, for example, the thermal evolution of oceanic lithosphere should follow half-space cooling before the onset of convection. See section 3.2 for further discussion on this point.

The use of equation (1) is equivalent to assuming no occurrence of sublithospheric convection, which we believe is adequate for the first 70 Myr of thermal evolution. Whereas some numerical studies suggest younger seafloor ages for the onset of sublithospheric, small-scale convection [e.g., Buck and Parmentier, 1986; Dumoulin *et al.*, 2001; Zlotnik *et al.*, 2008], the onset time depends critically on the rheology of the upper mantle [Korenaga and Jordan, 2002], our understanding of which is still limited [Korenaga and Karato, 2008; Mullet *et al.*, 2015]. Although there is a considerable time lag between the onset of sublithospheric convection and its manifestation in surface heat flow [Korenaga, 2009], the onset of convection would be immediately reflected in surface topography even with realistic mantle rheology [Korenaga, 2015]. As the global depth-age relation of seafloor does not exhibit notable deviations from the half-space cooling trend up to 70 Ma [Parsons and Sclater, 1977; Stein and Stein, 1992; Korenaga and Korenaga, 2008], the possibility of convective instability can be excluded when modeling the global behavior of young oceanic lithosphere. Note that this stance is not inconsistent with the earlier operation of small-scale convection on a regional scale.

In our modeling, the effect of melt extraction on mantle composition as well as equilibrium mineral assemblages are calculated using pMELTS simulations [Ghiorso *et al.*, 2002; Smith and Asimow, 2005; Asimow and Ghiorso, 1998], and mineral densities are computed based mainly on the compilation of Schutt and Lesher [2006]. The model incorporates 7 km thick oceanic crust, which is characterized by low density as well as low thermal diffusivity. The effect of radiative thermal conductivity [Hofmeister, 2005] is also considered for the mantle. The most realistic case we considered in this study (labeled as “+ crust + k_{rad} ” in figures) includes the effects of melt extraction, solid phase transitions, radiative thermal conductivity, and oceanic crust. We also considered four other auxiliary cases to quantify the magnitude of these different effects (see Table 1).

Table 1. Setting for Thermal Evolution Modeling

Label	Melt Extraction	Phase Changes	Radiative Thermal Conductivity	Oceanic Crust
+ crust + k_{rad}	Yes	Yes	Yes	Yes
+ crust	Yes	Yes	No	Yes
No crust	Yes	Yes	Yes	No
No phase change	Yes	No	Yes	Yes
Fo90 ^a	No	No	Yes	Yes

^aThe mantle is assumed to be made entirely of Fo₉₀ olivine.

In what follows, we will explain these effects in some detail, along with the description of how material properties, such as ρ , C_p , and k , vary with pressure and temperature.

2.1. Melt Extraction and Mantle Density

The partial melting of the mantle beneath mid-ocean ridges results in the chemical depletion of the residual solid, the effect of which is quantified through pMELTS simulations [Ghiorso *et al.*, 2002; Smith and Asimow, 2005]. For the source mantle composition, we used the primitive mantle composition model of Sun and McDonough [1989]; the effect of the extraction of continental crust is minimal on the major element composition of the mantle [e.g., Kinzler and Grove, 1992], allowing to use the primitive mantle as the present-day source mantle for mid-ocean ridge basalts. Isentropic melting was conducted starting from the initial pressure of 4 GPa and the initial temperature of 1723 K (1450°C) and assuming continuous melting with the minimum melt fraction of 0.2%. The composition of the residual mantle is shown at selected pressures in Table 2. The pMELTS simulation successfully produces ~7 km thick oceanic crust, and as shown in Table 3, the calculated composition of the accumulated melt phase resembles closely existing estimates on the primary melt composition for mid-ocean ridge basalts.

As shown in Figure A1, pMELTS predicts that the isentropic decompression of the mantle with the temperature of 1723 K (1450°C) at 4 GPa brings down the temperature to 1623 K (1350°C) at surface, if melting is suppressed (a similar result can also be seen in Figure 1 of Smith and Asimow [2005]). This corresponds to the adiabatic thermal gradient of 0.8 K km⁻¹, which is greater than typical values of ~0.5 K km⁻¹ [Langmuir *et al.*, 1992]. The source of this discrepancy is that both MELTS and pMELTS use the thermodynamic database of Berman [1988], which overpredicts the thermal expansivity of olivine at high pressures (Figure 1). Density values provided by pMELTS are thus not always reliable, and we chose to recalculate density based on the method of Schutt and Leshner [2006].

The compilation of Schutt and Leshner [2006] on thermodynamic quantities, however, does not cover all of mineral compositions given by our pMELTS simulations, so it is supplemented as follows. For spinel, Mg-chromite (MgCrO₄), magnetite (Fe₃O₄), qandilite (Mg₂TiO₄), and ulvospinel (Fe₂TiO₄) are added as end-member minerals. For feldspar, albite (NaAlSi₃O₈) and anorthite (CaAl₂Si₂O₈) are used as end-member minerals. Their relevant thermodynamic quantities are summarized in Table 4.

Table 2. Calculated Major Element Composition of the Mantle at Selected Pressures^a

Pressure	SiO ₂	TiO ₂	Al ₂ O ₃	Fe ₂ O ₃	Cr ₂ O ₃	FeO	MnO	MgO	NiO	CaO	Na ₂ O	F ^b
4 GPa ^c	44.92	0.20	4.44	0.12	0.38	7.93	0.13	37.73	0.25	3.54	0.36	0
2 GPa	44.92	0.20	4.40	0.12	0.38	7.93	0.13	37.81	0.25	3.54	0.33	0.17
1.5 GPa	44.89	0.17	4.12	0.12	0.37	7.92	0.13	38.39	0.26	3.45	0.17	2.48
1 GPa	44.74	0.12	3.44	0.11	0.41	7.93	0.14	39.78	0.27	3.04	0.03	7.47
0.5 GPa	43.71	0.01	0.97	0.07	0.47	8.26	0.16	45.16	0.32	0.97	0.00	22.18
0.18 GPa ^d	43.17	0.00	0.38	0.06	0.49	8.41	0.17	46.59	0.33	0.52	0.00	25.50

^aValues are in weight percent.

^bTotal fraction of melt removed.

^cSource mantle composition.

^dCorresponding to the base of the crust.

Table 3. Calculated and Estimated Primary Melt Compositions for Mid-Ocean Ridge Basalts^a

Source	SiO ₂	TiO ₂	Al ₂ O ₃	Fe ₂ O ₃	Cr ₂ O ₃	FeO	MnO	MgO	NiO	CaO	Na ₂ O
This study	48.57	0.93	16.34	0.23	0.08	7.19	0.01	12.72	0.01	11.26	2.65
Kinzler [1997] ^b	48.20	0.94	16.40	0.00	0.12	7.96	0.00	12.50	0.00	11.40	2.27
Korenaga and Kelemen [2000] ^c	48.80	0.97	16.20	0.50	0.00	7.80	0.12	12.40	0.01	10.80	2.40
Herzberg and O'Hara [2002] ^d	48.40	0.84	16.40	0.56	0.00	7.40	0.12	12.70	0.00	11.30	2.25

^aValues are in weight percent.

^bEstimate based on polybaric, near-fractional melting with the initial pressure of 1.5 GPa.

^cEstimate based on multiphase fractionation correction to samples from northern East Pacific Rise.

^dEstimate using a sample from the Siqueros transform fault, assuming the accumulated perfect fractional melting of depleted source mantle.

2.2. Phase Transitions

After its ascent beneath a mid-ocean ridge, the mantle is cooled from the above and is assumed to move only laterally. During this phase, the chemical composition of the mantle is a simple function of pressure (or depth), but equilibrium mineral assemblages at a particular pressure can still vary with changes in temperature. We use pMELTS to track such variations in mineral assemblages and calculate corresponding densities using the method of Schutt and Lesher [2006] as mentioned above (Figure 2). In consideration of how pMELTS has been calibrated, the calculation of equilibrium mineral assemblages by pMELTS was limited to pressures lower than 4 GPa and temperatures above 800 K, and extrapolations to higher pressures and lower temperatures were made for mineral assemblages using the nearest neighbor algorithm. In the case of “no phase change,” the equilibrium mineral assemblages before any cooling (i.e., right beneath a mid-ocean ridge) are used at all

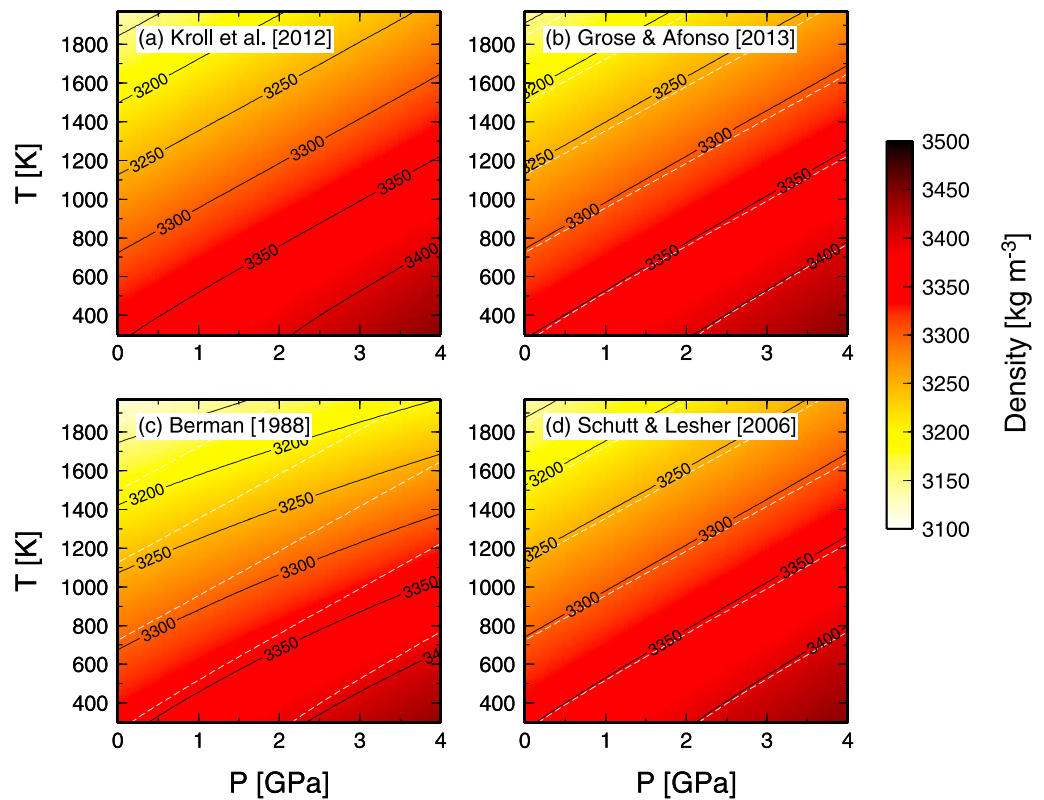


Figure 1. Density of Fo₉₀ olivine as a function of pressure and temperature, based on (a) the formulation of Kroll *et al.* [2012], which is based on so far the most complete compilation of thermal expansivity measurements as well as the up-to-date summary of bulk modulus data; (b) the formulation of Grose and Afonso [2013], which is based on the thermal expansivity of pure forsterite [Bouhifd *et al.*, 1996] and the isothermal bulk modulus of 130 GPa at room temperature and pressure with its pressure derivative K_T' of 4.8 and the Anderson-Grüneisen parameter δ_T of 6; (c) the formulation of Berman [1988]; and (d) the formulation of Schutt and Lesher [2006]. Dashed contours in Figures 1b–1d denote the prediction based on Kroll *et al.* [2012] shown in Figure 1a.

Table 4. Thermodynamic Quantities Adopted for Additional End-Member Minerals^a

Mineral	ρ_0^b (kg m ⁻³)	$K_{T,0}^c$ (GPa)	dK/dP	dK/dT (GPa K ⁻¹)	a_0	a_1	a_2
Mg-chromite	4414 ^d	182.5 ^f	5.8 ^f	-0.02 ^j	0.143 ^l	1.119 ^l	-0.1063 ^l
Magnetite	5200 ^d	222 ^g	4.1 ^g	-0.02 ^j	0.635 ^m	-0.7406 ^m	-4.467 ^m
Qandilite	3535 ^e	172 ^e	4 ^e	-0.02 ^j	0.2115 ⁿ	1.4546 ⁿ	0.3403 ⁿ
Ulvospinel	4775 ^d	222 ^h	4.1 ^h	-0.02 ^j	0.635 ^h	-0.7406 ^h	-4.467 ^h
Albite	2615 ^d	57.6 ⁱ	4 ⁱ	-0.02 ^k	- ^o	- ^o	- ^o
Anorthite	2765 ^d	81.6 ⁱ	4 ⁱ	-0.02 ^k	- ^o	- ^o	- ^o

^aThermal expansivity is calculated as $\alpha = a_0 \times 10^{-4} + a_1 \times 10^{-8}T + a_2/T$, unless noted otherwise.

^bDensity at the standard condition (298 K and 10⁵ Pa).

^cIsothermal bulk modulus at the standard condition.

^d*Smyth and McCormick* [1995, 1995].

^e*Lv et al.* [2016].

^f*Nestola et al.* [2014].

^g*Haavik et al.* [2000].

^hAssumed to be the same as magnetite.

ⁱ*Angel* [2004].

^jAssumed.

^k*Tribaudino et al.* [2011].

^l*Fei* [1995].

^mA single equation fit to the two equations reported by *Fei* [1995] (for < 843 K and > 843 K).

ⁿA fit to the formulation of *O'Neill et al.* [2003].

^oFollowing *Tribaudino et al.* [2010], the thermal expansivity of plagioclase is calculated as $b_0 + 2b_1(T - 298)$, where $b_0 = 2.44 \times 10^{-5} - 3.1 \times 10^{-7}x_{An} + 1.8 \times 10^{-9}x_{An}^2$, $b_1 = 9 \times 10^{-9} - 4 \times 10^{-11}x_{An}$, and x_{An} is the mole fraction of anorthite in percent.

pressures and temperatures, and in the case of “Fo90,” the mantle is assumed to be made entirely of Fo₉₀ olivine. Even with constant mineral assemblages, in situ density still varies with pressure and temperature through compressibility and thermal expansivity (Figure 1).

To quantify the “true” buoyancy of oceanic lithosphere, it would be convenient to use the concept of “potential density” (Appendix A). To calculate potential density at 4 GPa (ρ_{p4}), we first use pMELTS to calculate equilibrium assemblages at the pressure of 4 GPa and a range of temperatures, for the range of mantle composition resulting from melting, and calculate corresponding densities using the method of *Schutt and Leshner* [2006] (Figure 3). The potential density ρ_{p4} may then be found by calculating the corresponding potential temperature T_{p4} .

2.3. Specific Heat and Thermal Conductivity

Just as density, specific heat is also the function of pressure, temperature, and composition, but regarding their influence on the thermal evolution of the suboceanic upper mantle, it is a good approximation to consider only its temperature dependency. By compiling all of pMELTS simulation results obtained in this study, we found that the specific heat of the mantle can be approximated as

$$C_p(T) = 1580 - 12230T^{-0.5} - 1694 \times 10^6 T^{-3}, \quad (2)$$

where specific heat is in J K⁻¹ kg⁻¹.

For thermal conductivity, we adopt the approach of *Grose and Afonso* [2013] and first calculate thermal diffusivity as

$$\kappa(T) = \left[a + b \exp\left(-\frac{T-273}{c}\right) + d \exp\left(-\frac{T-273}{e}\right) \right] \times 10^{-6}, \quad (3)$$

where diffusivity is in m² s⁻¹, $a = 0.565$, $b = 0.67$, $c = 590$, $d = 1.4$, and $e = 135$. Thermal conductivity is then calculated as

$$k(P, T) = \kappa(T)C_p(T)\rho(P, T) \exp\left(\frac{d \ln(k)}{dP}P\right), \quad (4)$$

where $d \ln(k)/dP$ is set to 0.05 GPa⁻¹ [*Hofmeister*, 2007]. When radiative conductivity is considered in our modeling, we add the radiative contribution to the above conductivity, using the formulation of *Hofmeister* [2005], assuming the grain size of 5 mm.

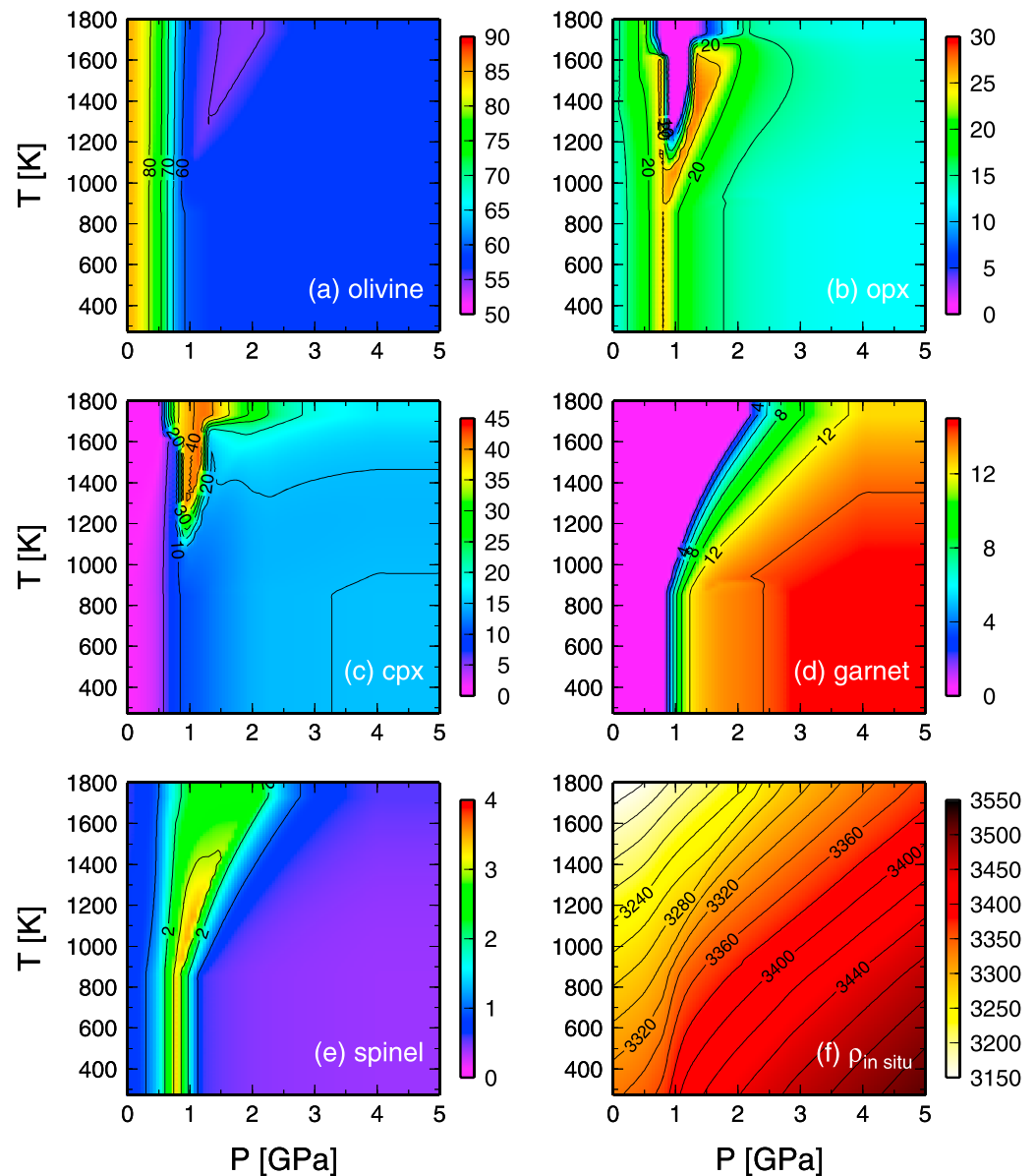


Figure 2. (a–e) Volume percentage of equilibrium mineral assemblages for suboceanic mantle as a function of pressure and temperature and (f) corresponding in situ mantle density. Variations in the mineral assemblage also reflects the effect of melt extraction.

2.4. Oceanic Crust

When 7 km thick oceanic crust is included in our modeling, we assume the same thermodynamic properties of the crust as used by *Grose and Afonso* [2013]. For this limited depth extent, modeling its detailed behavior is not very important, and the major impact of the crustal layer is limited to the following two aspects: its low reference density (2950 kg m^{-3}), which contributes significantly to the buoyancy of oceanic plates, and its low thermal diffusivity ($\sim 0.6 \times 10^{-6} \text{ m}^2 \text{ s}^{-1}$ on average), which tends to insulate the underlying mantle section.

3. Results and Discussion

3.1. On Excess Density of the Cooling Lithosphere

Modeling results for the most realistic case, with the effects of melt extraction, solid phase transition, oceanic crust, and radiative thermal conductivity, are shown in Figure 4. Despite the intricacy of modeled thermal properties, the growth of the cold boundary layer still follows closely the prediction of simple half-space cooling (Figure 4a). In contrast, the corresponding in situ density is more complex, affected not only by

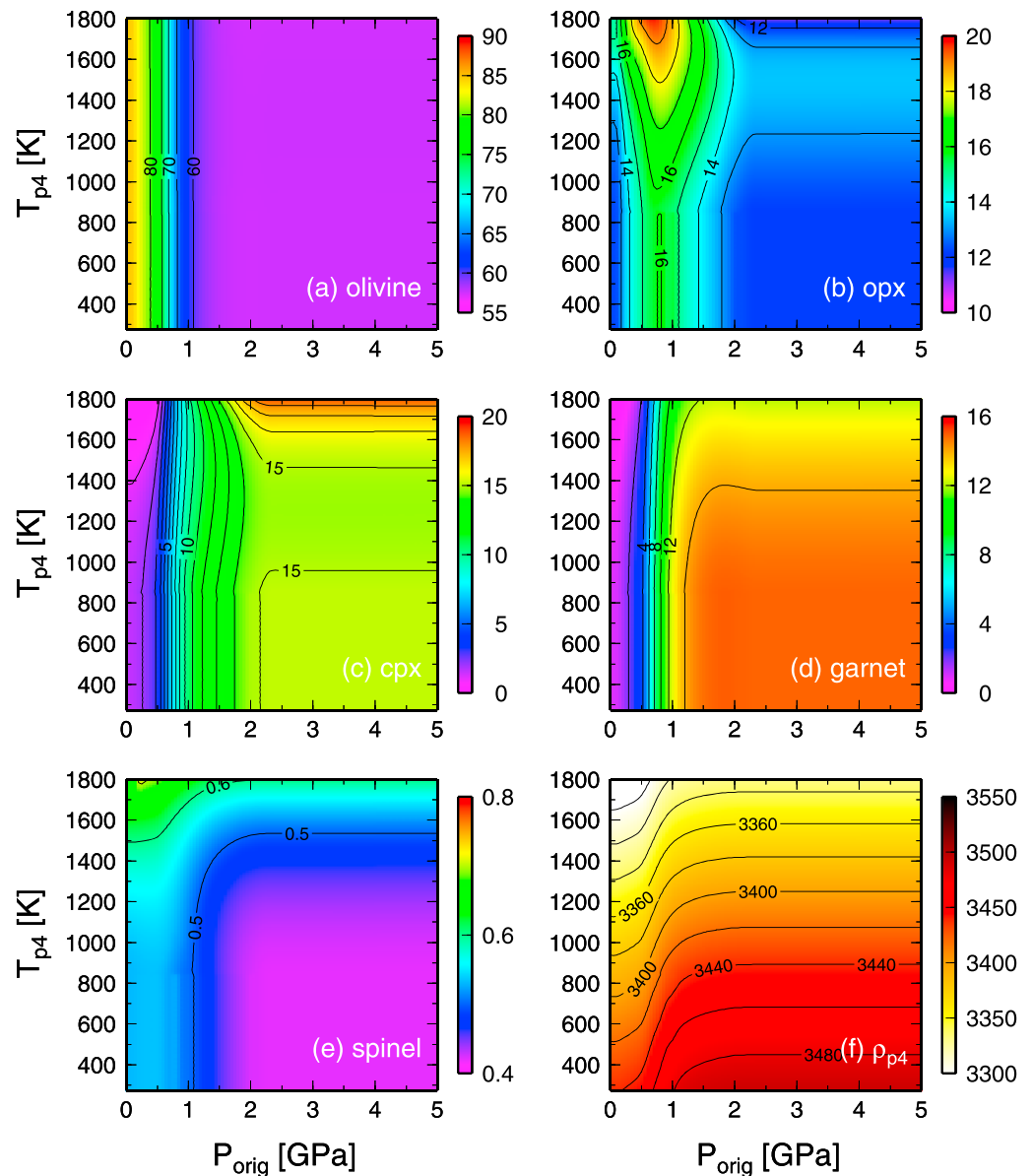


Figure 3. (a–e) Volume percentage of equilibrium mineral assemblages at 4 GPa as a function of original pressure and temperature and (f) corresponding potential mantle density. Lack of pressure sensitivity at $P > 2$ GPa results simply from that the mantle composition is the same before melting starts.

changes in temperature and pressure but also by variations in chemical composition and mineral assemblages (Figure 4b). Conversion to the potential density ρ_{p4} (Appendix A), however, reveals a dynamically more meaningful picture of density stratification, which evolves simply with the growth of the cold boundary layer (Figure 4c). The depth profile of in situ density may give an impression that the top 100 km of suboceanic mantle does not become denser than the underlying mantle even after 90 Myr of cooling (Figure 4d), and this in fact underlies the suggestion of mature yet buoyant oceanic lithosphere [Hynes, 2005; Valencia *et al.*, 2007; Valencia and O’Connell, 2009]. The previous calculation of the temporal evolution of in situ density [e.g., Hynes, 2005] is not considerably different from ours; it is its physical interpretation that has been confounded. By calculating ρ_{p4} , we can correct for the effect of isentropic compression, and the chemical buoyancy of the depleted lithospheric mantle is seen to be compensated quickly, within the first 10 Myr (Figures 4c and 4d). Even with the buoyant basaltic crust, the net buoyancy of suboceanic mantle becomes negative after ~ 30 Myr (Figure 5a), which is only slightly greater than the conventional estimate of 20 Myr

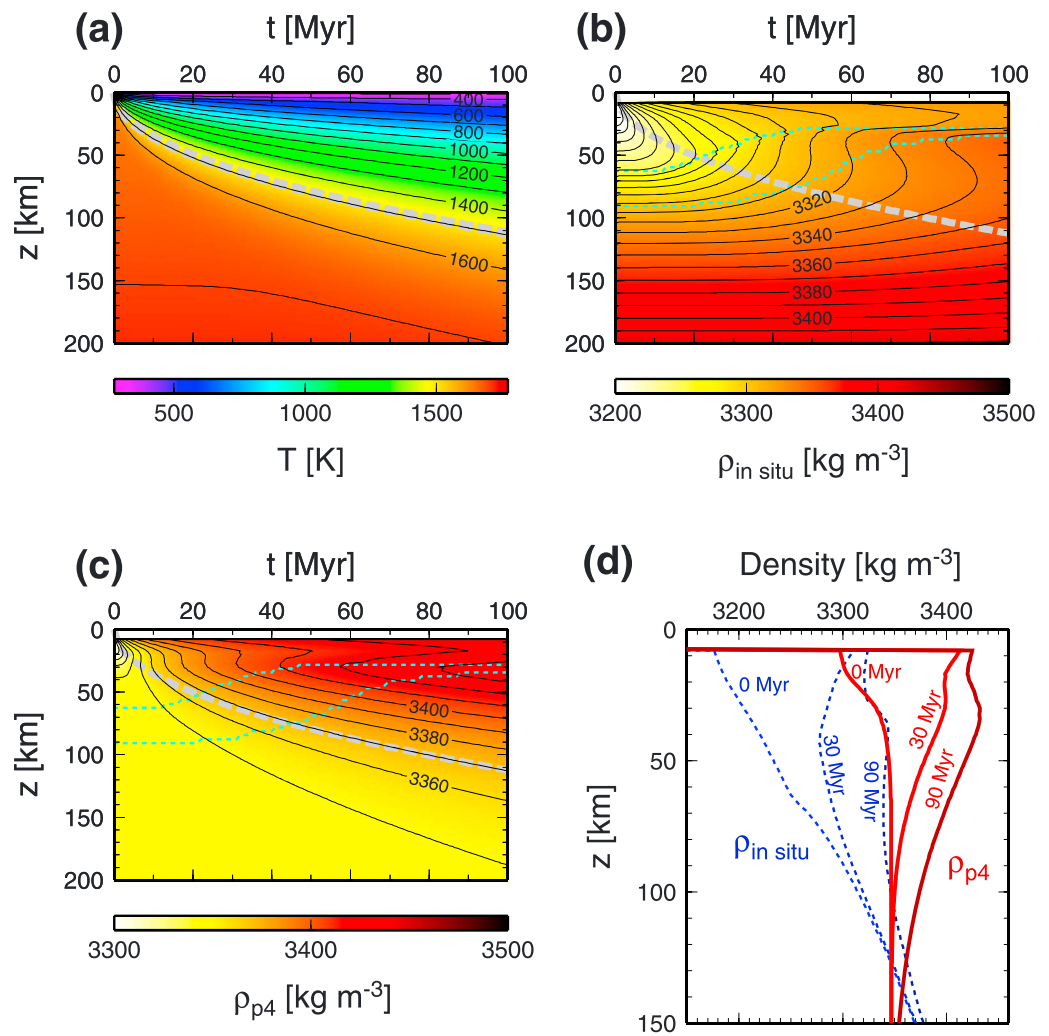


Figure 4. The thermal evolution modeling with the effects of melt extraction, solid phase transitions, radiative thermal conductivity, and 7 km thick oceanic crust. The total model depth is 300 km, which is sufficiently deep to model half-space cooling for the duration of 100 Myr, but only the shallow portion is shown here for clarity. (a) In situ temperature, (b) in situ density, and (c) potential density at 4 GPa. Gray dashed line in those panels denotes the extent of the classical thermal boundary layer defined by $2\sqrt{\kappa t}$, where κ is thermal diffusivity (here fixed to be $10^{-6} \text{ m}^2 \text{ s}^{-1}$) and t is time. Blue dotted curves in Figures 4b and 4c represent the spinel-to-garnet phase transition: the volume fraction of garnet is less than 1% above the upper curve and above 10% below the lower curve. (d) The profiles of in situ density (dotted) and potential density (solid) are shown at 0, 30, and 90 Myr.

[Davies, 1992]. The subduction of an oceanic plate could therefore take place by its own gravitational instability, resolving the aforementioned causality dilemma of plate tectonics.

Note that whereas Valencia *et al.* [2007] and Valencia and O'Connell [2009] cite the work of Afonso *et al.* [2007], in addition to that of Hynes [2005], to argue for the potential insignificance of plate's own buoyancy for the operation of plate tectonics, Afonso *et al.* [2007] themselves do not misinterpret their computed profile of in situ density, unlike Hynes [2005]. From Figure 3 of Afonso *et al.* [2007], one can deduce that their model also predicts that the oceanic lithosphere becomes negatively buoyant after ~ 30 Myr. The agreement between Afonso *et al.* [2007] and our study is encouraging because these studies employ different implementations for petrological and geophysical modeling.

3.2. Predicted Rates of Seafloor Subsidence

Model predictions for surface heat flow are similar among all cases considered (Figure 5b), satisfying observations equally well. Seafloor subsidence proves to be a more discriminating observable (Figure 5c). As shown

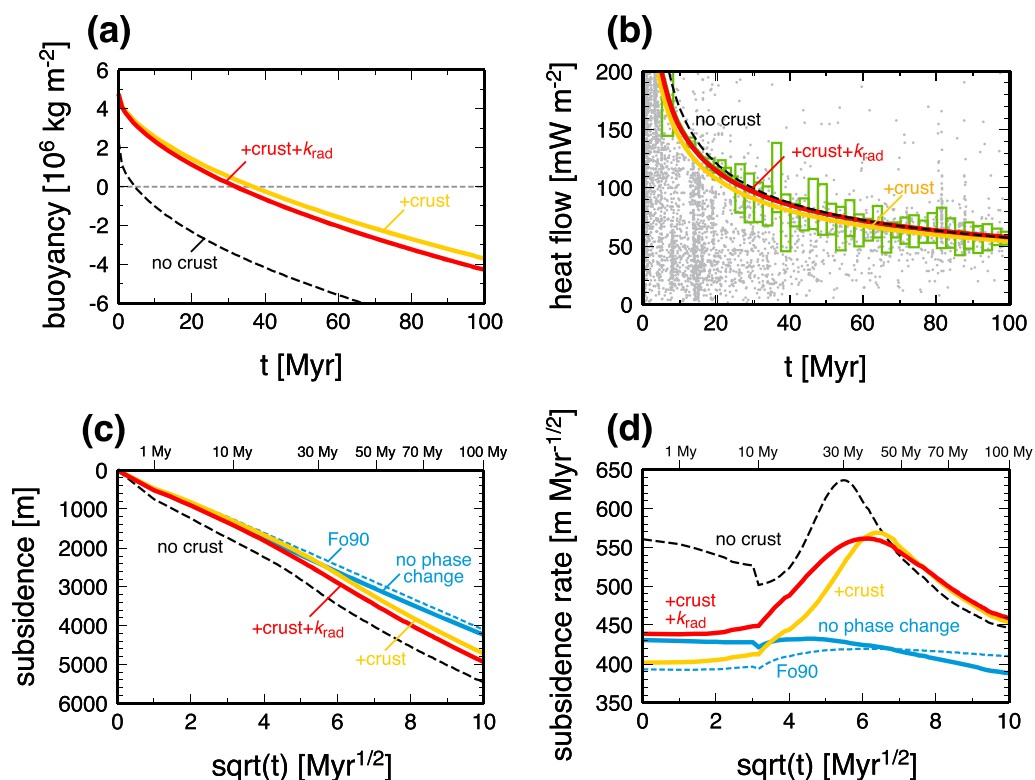


Figure 5. Comparison of five different models in terms of buoyancy, heat flow, and subsidence. Results for the most complete model, which incorporates the effects of melt extraction, solid phase transition, radiative thermal conductivity, and oceanic crust, are labeled as + crust + k_{rad} and shown in red. All other models are missing one or more factors as follows: without radiative thermal conductivity (“+ crust”; yellow), without radiative thermal conductivity and oceanic crust (“no crust”; dashed black), without solid phase transition (no phase change; blue), and the model without melt extraction and solid phase transition (Fo90; dashed blue). (a) Evolution of the net buoyancy of suboceanic mantle, defined as $\int_0^{z_{\text{max}}} [\rho_{p4}(t, z) - \rho_{p4}(0, z_{\text{max}})] dz$, where z_{max} is 300 km. (b) Evolution of surface heat flux. Gray dots shows all of available heat flow data [International Heat Flow Commission of IASPEI, 2011] from the normal seafloor [Korenaga and Korenaga, 2008]. Green boxes denote the recent compilation [Hasterok, 2013]. In Figures 5a and 5b, the cases of no phase change and Fo90 are virtually identical to the most complete case. (c) Seafloor subsidence plotted as a function of square root of time. (d) Rate of seafloor subsidence calculated by linear regression using a moving window of ± 10 Myr.

previously [Grose and Afonso, 2013], the presence of low-thermal-diffusivity crust tends to insulate the mantle, thereby slowing down seafloor subsidence. The addition of radiative thermal conductivity has an opposite effect albeit of smaller magnitude. The average subsidence rate for the first 70 Myr is $\sim 500 \text{ m Myr}^{-1/2}$ for the most realistic case (red curve in Figure 5d). When phase change is artificially suppressed (blue curve in Figure 5d), the average rate would reduce to $\sim 420 \text{ m Myr}^{-1/2}$, so the spinel-to-garnet transition in the cooling lithosphere contributes $\sim 80 \text{ m Myr}^{-1/2}$ of extra subsidence. The observed subsidence rate for the normal seafloor, i.e., the seafloor unaffected by the emplacement of oceanic islands and oceanic plateaus, is only $\sim 320 \text{ m Myr}^{-1/2}$ [Korenaga and Korenaga, 2008]. Our calculation of isostatic adjustment correctly incorporates the effect of compressibility, which minimizes the magnitude of subsidence (Appendix B). The substantial discrepancy between the theoretical prediction and the observation thus seems to require the operation of some mechanisms unaccounted in our modeling. The 84% ($420 \text{ m Myr}^{-1/2}$) and 16% ($80 \text{ m Myr}^{-1/2}$) of the total predicted subsidence ($500 \text{ m Myr}^{-1/2}$) are caused by thermal contraction and phase transition, respectively, and there is no known mechanism to reduce the contribution from the phase transition. To explain the observed subsidence rate of $\sim 320 \text{ m Myr}^{-1/2}$, therefore, the subsidence caused by thermal contraction has to be reduced down to $240 \text{ m Myr}^{-1/2}$, i.e., $\sim 40\%$ decrease.

The predicted subsidence rate of $\sim 500 \text{ m Myr}^{-1/2}$ may seem exceedingly high, but lower, traditional predictions are based primarily on the use of thermal expansivity that is too low to be compatible with

mineral physics. A simple model of thermal isostasy with constant material properties yields the following formula for subsidence rate:

$$\frac{dw}{dt} = \frac{2\alpha\rho_m\Delta T\sqrt{\kappa/\pi}}{\rho_m - \rho_w}, \quad (5)$$

where α is thermal expansivity, ΔT is the difference between the surface temperature and the initial mantle temperature, κ is thermal diffusivity, ρ_m is mantle density, and ρ_w is water density [Turcotte and Schubert, 1982]. Using $\alpha = 3 \times 10^{-5} \text{ K}^{-1}$, $\kappa = 10^{-6} \text{ m}^2 \text{ s}^{-1}$, $\rho_m = 3300 \text{ kg m}^{-3}$, and $\rho_w = 1000 \text{ kg m}^{-3}$, the subsidence rate is predicted to be $\sim 355 \text{ m Myr}^{-1/2}$ for $\Delta T = 1300 \text{ K}$. This subsidence rate is close enough to the estimate of Carlson and Johnson [1994] for the normal subsidence rate ($345 \pm 3 \text{ m Myr}^{-1/2}$), so theory and observations seem to agree well. Even with this simple formula, however, the subsidence rate becomes $\sim 430 \text{ m Myr}^{-1/2}$ by using $\alpha = 3.5 \times 10^{-5} \text{ K}^{-1}$, which is more compatible with mineral physics measurements, and using $\Delta T = 1350 \text{ K}$, which is more consistent with the petrology of mid-ocean ridge basalts [Herzberg et al., 2007]. The effect of the spinel-to-garnet transition, which is not considered in equation (5), further increases the subsidence rate by $\sim 80 \text{ m Myr}^{-1/2}$ as discussed above.

The case Fo90, in which the mantle is assumed to be made entirely of Fo₉₀ olivine, is most similar to the model of Grose and Afonso [2013], which also yields a predicted subsidence rate higher than the observed (around $390 \text{ m Myr}^{-1/2}$). The subsidence rate for the case Fo90 is slightly higher than this, reaching $410 \text{ m Myr}^{-1/2}$ after the first 30 Myr (Figure 5d). As mentioned in section 2, Grose and Afonso [2013] adopted the plate model and fixed the model temperature at a relatively shallow depth ($\sim 100 \text{ km}$). Even if we restrict ourselves for the early evolution of oceanic lithosphere, the influence of this bottom boundary condition is not entirely absent. As one can see most clearly in Figure 4c, the cooling front reaches to the depth of 100 km only after 30 Myr. The use of the plate model is therefore the likely source of this small discrepancy between the case Fo90 and the model of Grose and Afonso [2013]. In addition to using the plate model, which helps to explain the subsidence of old seafloor, Grose and Afonso [2013] reduced thermal expansivity to fit the subsidence of young seafloor. We do not adopt the plate model as it hinders our effort to understand seafloor subsidence in a dynamically meaningful manner [Korenaga, 2015], and by the same token, we would like to identify physically plausible mechanisms that can explain the discrepancy between the predicted and observed subsidence rates. This will be discussed in the next section.

3.3. Other Mechanisms That May Contribute to Subsidence Rates

It is known that thermal contraction cannot take place freely when viscosity depends strongly on temperature [Korenaga, 2007a]. Full thermal contraction can be achieved only at the limit of complete viscous relaxation, the approach to which is prevented when viscosity becomes too high at low temperatures. This incomplete viscous relaxation also generates high thermal stress, which leads to the pervasive thermal cracking of oceanic lithosphere [Korenaga, 2007b]; this situation is akin to cracking hot glassware with cold water. The consequence of incomplete viscous relaxation and thermal cracking can be expressed collectively as effective thermal expansivity, and with the typical activation energy for the viscosity of olivine aggregates ($\sim 300\text{--}500 \text{ kJ mol}^{-1}$ [e.g., Hirth and Kohlstedt, 2003]), the effective thermal expansivity of oceanic lithosphere can be reduced by up to $\sim 20\%$ [Korenaga, 2007a]. The effect of incomplete viscous relaxation is applicable only to the thermal contraction part of subsidence, and with the maximum 20% reduction in thermal expansivity, the total subsidence, including the effect of phase transition, could be reduced only down to $\sim 416 \text{ m Myr}^{-1/2}$, which is still $\sim 30\%$ higher than the observed rate.

Seafloor subsidence can also be affected by a slight temperature gradient in the convecting mantle produced by radiogenic heat production [Korenaga, 2015]. The amount of heat-producing elements such as U and Th in the convecting mantle is very small, with the estimate of their total heat production being on the order of $1\text{--}3 \times 10^{-12} \text{ W kg}^{-1}$ (equivalent to $4\text{--}12 \text{ TW}$ for the entire mantle) [Jochem et al., 1983; Korenaga, 2008], which would lead to only $<10 \text{ K}$ increase over 100 Myr. Still, as opposed to more random fluctuations in the mantle temperature, a systematic temperature trend created by internal heat generation results in age-dependent dynamic topography, which in turn affects the global subsidence rate. This effect can be amplified further by the secular cooling of the mantle, which is estimated to be $\sim 100 \text{ K Gyr}^{-1}$ over the Phanerozoic [Herzberg et al., 2010]. The combined influence of internal heating and secular cooling is quantified through the fluid-dynamical calculation of surface topography (Appendix C). Surface topography is sensitive to the mantle viscosity structure, and representative results are summarized in Figures 6a and 6b. The total internal heating

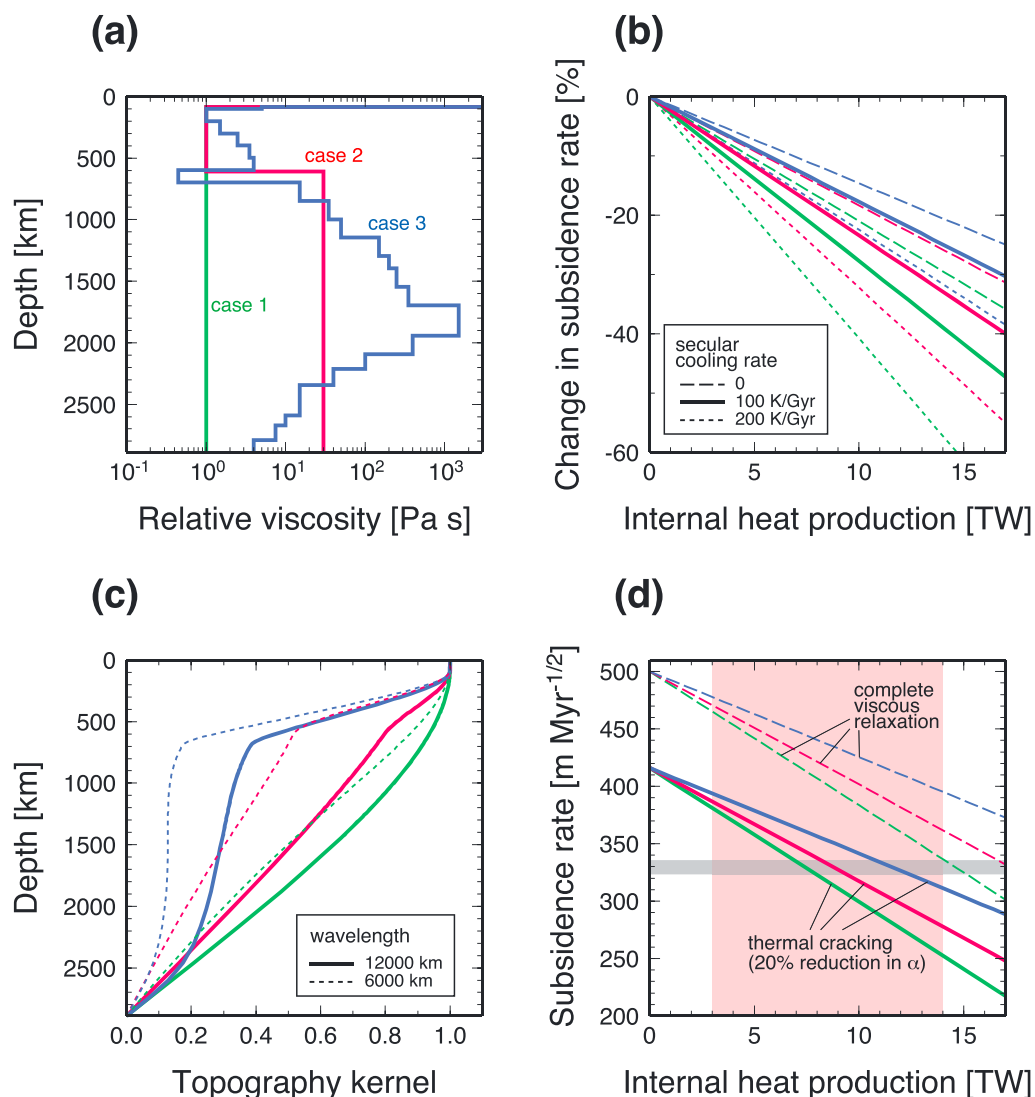


Figure 6. (a) Three viscosity profiles used for the calculation of surface topography. Case 1 (green): Purely temperature-dependent viscosity, i.e., without intrinsic viscosity change with depth. Case 2 (red): Similar to case 1 but with thirtyfold increase for the lower mantle. Case 3 (blue): More complicated depth dependency resembling the model of *Mitrovica and Forte* [2004]. Line colors used in Figures 6b–6d correspond to these viscosity profiles. (b) Change in subsidence rate caused by internal heat production, with three different secular cooling rates: 0 K Gyr⁻¹ (dashed), 100 K Gyr⁻¹ (solid), and 200 K Gyr⁻¹ (dotted). (c) Surface topography kernel at the horizontal wavelength of 12000 km (solid) and 6000 km (dotted). (d) Subsidence rate prediction as a function of internal heat production, with complete viscous relaxation (dashed) and with incomplete relaxation and thermal cracking (solid). Gray horizontal shading denotes the range of estimated global subsidence rate (323 to 336 m Myr^{-1/2}, depending on the definition of normal seafloor [*Korenaga and Korenaga, 2008*]), and pink vertical shading represents geochemical constraints on internal heat production in the convecting mantle (8.5 ± 5.5 TW [*Korenaga, 2008*]).

of 10 TW with the secular cooling rate of 100 K Gyr⁻¹, for example, can reduce the subsidence rate by ~20%. The sensitivity of seafloor subsidence to the minute temperature variation in the deep convecting mantle may be best appreciated by the surface topography kernel [*Parsons and Daly, 1983*] (Figure 6c). Density anomalies at different depths contribute differently to surface topography, usually with greater contributions from shallower anomalies. Isostasy with an arbitrary depth of compensation (typically set to 200–300 km) is equivalent to assuming the topography kernel being unity above the compensation depth and zero below it, but in reality, the topography kernel has more gradual depth dependency, and deep density anomalies can still affect surface topography. Figure 6c indicates that at ocean-wide spatial scales, density variations even at the depth of 2000 km can have a nontrivial effect on surface topography. The effects of internal heating and

secular cooling on subsidence rate are entirely independent from that of reduced thermal expansivity, and their combined effect is shown in Figure 6d. Neither effect alone is sufficient to explain the observed subsidence rate, and their combination seems essential to comply with geochemical constraints on the amount of heat-producing elements in the convecting mantle.

4. Conclusion and Outlook

Our integrated geophysical and petrological modeling represents by far the most complete treatment of the evolution of young oceanic lithosphere. The use of potential density allows us to correctly interpret the dynamical meaning of the resulting density structure, and oceanic lithosphere is shown to become negatively buoyant with respect to the underlying asthenosphere after ~ 30 Myr. The buoyancy criterion for the initiation of subduction is thus resurrected, helping to demystify the dynamics of plate tectonics. As the operation of plate tectonics is commonly believed to be vital for planetary habitability [Kasting and Catling, 2003], this clarification will be important also for the evolution of exoplanets [Valencia et al., 2007; Korenaga, 2013]. At the same time, our modeling suggests that the seafloor subsidence is a phenomenon considerably more involved than is usually thought. The observed subsidence rate is too low to be compatible with the thermal expansivity of mantle minerals, and the situation is aggravated further by the spinel-to-garnet transition. It is rather remarkable that by including all of often overlooked yet physically plausible effects, i.e., incomplete viscous relaxation within oceanic plates, radiogenic heat production in the convecting mantle, and the secular cooling of the Earth, the discrepancy between the theoretical prediction and the observation is just resolved.

As indicated in section 2.1, however, our implementation of relevant thermodynamics is not entirely self-consistent because the thermal expansivity data used in the calibration of pMELTS are somewhat outdated and are not appropriate for the purpose of calculating isostasy; isostasy reflects integrated mass anomalies, and small deviations can add up to a substantial difference. Therefore, it will be important to test the robustness of our conclusions by comparing results with different thermodynamic implementations [e.g., Holland and Powell, 1998; Stixrude and Lithgow-Bertelloni, 2005, 2011].

This study concerns only the present-day situation, and its application to the past conditions remains to be seen. Hotter mantle and more radiogenic heating in the past should have increased, respectively, the extent of chemical buoyancy and the magnitude of dynamic topography. Such consideration will be indispensable when considering the likelihood of plate tectonics, along with its influence on surface environment via sea level changes, throughout the Earth history. We have adopted one particular source mantle composition in this study, but testing different composition models [e.g., Hart and Zindler, 1986; Palme and O'Neill, 2003; Lyubetskaya and Korenaga, 2007] is warranted when assessing the effect of elevated mantle temperature.

Appendix A: Potential Density

Potential density is widely used in oceanography and atmospheric science but much less so in solid earth sciences. The potential density of a material is a hypothetical density that the material would acquire if isentropically brought to a reference pressure. The use of potential density is essential when considering density stratification in a compressible medium. When a material is isentropically brought down to a greater depth, for example, its temperature and density both increase, so when comparing densities at different depths, we always need to take into account this density variation along an adiabat, and potential density is used for this purpose. As seen in Figure A1, the choice of reference pressure is important for potential density. If we choose the surface pressure as a reference, as usually done for potential temperature [e.g., McKenzie and Bickle, 1988], garnet and spinel in the undepleted asthenospheric mantle would transform to plagioclase, making the undepleted mantle more buoyant than the depleted one that has exhausted those aluminum-bearing phases by melting. Because we are interested in whether the shallow depleted mantle can become denser than the asthenosphere so that it can sink deeper, it is better to take a reference pressure somewhere below major phase transitions. We use the reference pressure of 4 GPa in this study and denote the corresponding potential temperature and density as T_{p4} and ρ_{p4} , respectively.

Some may find it difficult to understand why the choice of the reference pressure matters, but this is because the mantle can melt as well as undergo solid phase transitions during isentropic decompression. Following the convention for potential temperature in igneous petrology, we suppress melting along isentropic paths

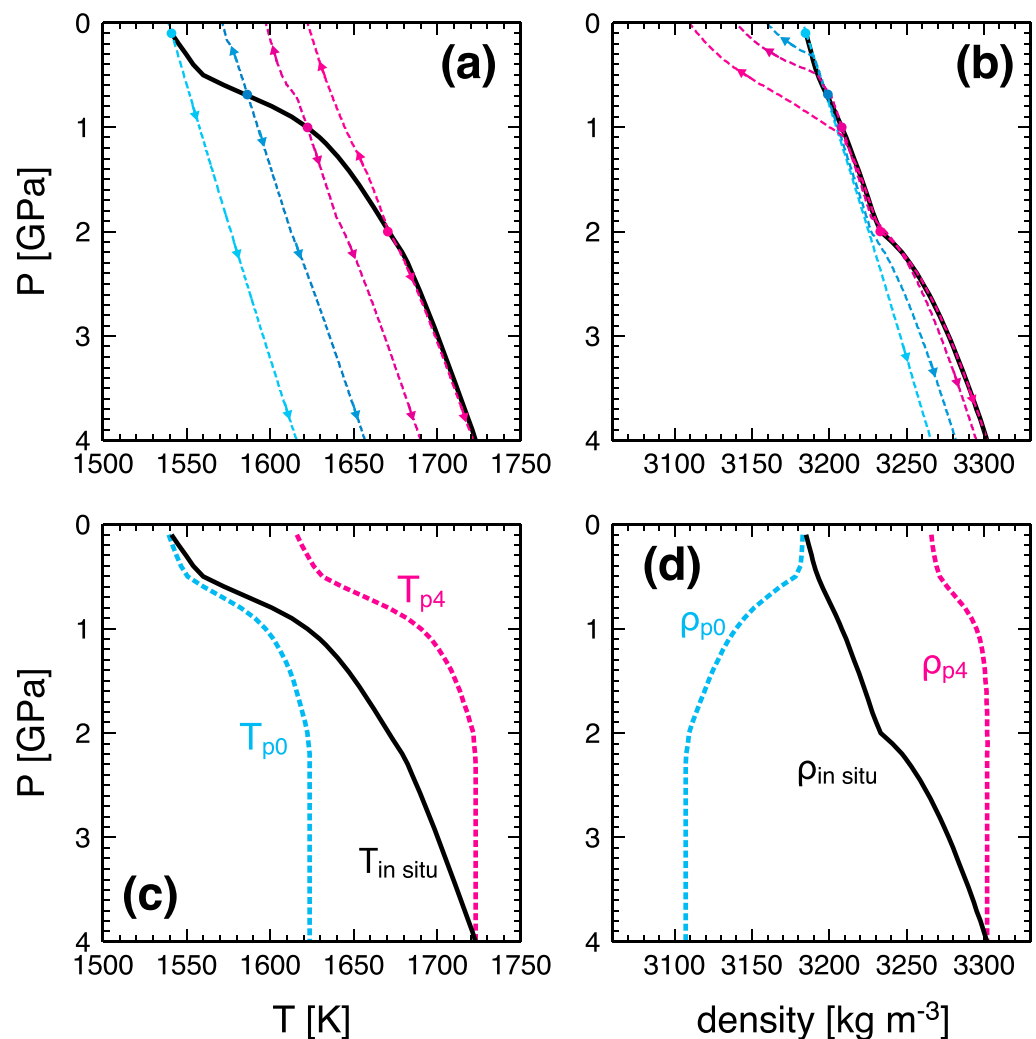


Figure A1. The concept of potential temperature and density. In all panels, thick curves denote either (a and c) in situ temperature or (b and d) in situ density for the mantle beneath a mid-ocean ridge with the potential temperature of 1623 K (1350°C). The in situ temperature profile reflects cooling due to isentropic decompression as well as the release of latent heat of fusion. In Figures A1a and A1b, dashed curves show how temperature and density vary with isentropic decompression (upgoing) and compression (downgoing). As with the convention for potential temperature, melting is suppressed during those isentropic paths, though solid phase transitions still take place; a kink in the density profile at ~2 GPa is caused by the spinel-to-garnet transition. In Figure A1c, dashed curves show the potential temperature referenced at the surface (blue) and at 4 GPa (red). Potential density is shown in Figure A1d in a similar manner. The effect of melt depletion on mantle density is best seen in the profile of ρ_{p4} . With the potential temperature of 1623 K, melting starts at ~2 GPa, but its effect on mantle density becomes notable only for <1 GPa. These temperature and density profiles are taken directly from pMELTS simulations, so isentropic thermal gradients are slightly too large to be compatible with more recent compilations of thermodynamic data (see section 2.1).

but still allow solid phase transitions, and we need to choose the reference pressure for it to be useful for our discussion. Even when a material under consideration does not experience phase transition of any kind, the choice of the reference pressure can be important, and this is in fact the case in oceanography, because of the complicated and nonlinear equation of state for sea water [e.g., Pond and Pickard, 1983]. In oceanography, therefore, it is necessary to evaluate a local stability as a function of depth. Such a comprehensive approach is not demanded in our case, because we are primarily interested in knowing whether the lithosphere is denser than the underlying asthenosphere, when the lithosphere is brought down to the same depth of the asthenosphere. As long as we move downward along isentropic paths (i.e., isentropic compression), no further melting would take place even if we do not suppress melting, so the potential density defined at 4 GPa can directly be used to assess the subductability of lithosphere.

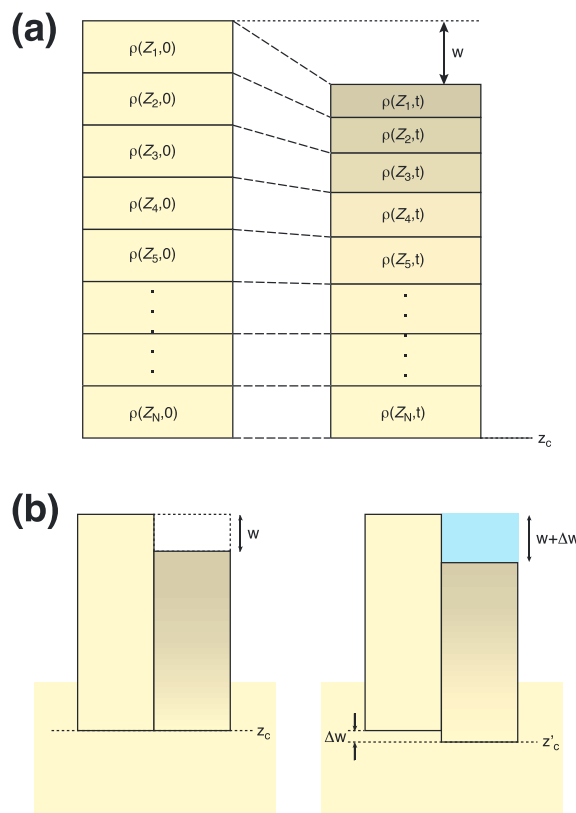


Figure B1. (a) Thermal isostasy as vertical thermal contraction. Density is described here as a function of Z_i , which is the Lagrangian coordinate in the vertical direction, and time t . The amount of subsidence and the depth of compensation are denoted by w and z_c , respectively. (b) Effect of water on isostatic adjustment. Extra subsidence of Δw displaces the depth of compensation to z'_c .

Appendix B: Thermal Isostasy With a Compressible Medium

Whereas thermal isostasy is a well-known concept [e.g., *Turcotte and Schubert, 1982*], it is difficult to find in the literature its correct formula when a material is compressible, so we will derive it in the following.

The problem of thermal isostasy may be understood simply as thermal contraction in the vertical direction, and the situation is the simplest when the overlying medium is air, the density of which can be neglected (Figure B1a). Using the Lagrangian coordinate Z , which shrinks with contraction, the total subsidence w at time t may be expressed as

$$w = \int_0^\infty \left(1 - \frac{\rho(Z', 0)}{\rho(Z', t)} \right) dZ', \quad (B1)$$

where the original coordinate at $t=0$ is assumed in the integration. The original density $\rho(Z', 0)$ can vary with depth, so this formulation is sufficiently general to handle a compressible medium. The upper limit of the integral is ∞ , but in reality, $\rho(Z', t) = \rho(Z', 0)$ at sufficiently great depths where cooling has not reached, and the depth of compensation may be placed at the minimum depth where such equality holds.

In case that densities before and after thermal contraction are both constant as ρ_m and ρ_L , respectively, and the length of the contracted column is L , the above equation is reduced to

$$w = \left(1 - \frac{\rho_m}{\rho_L} \right) (L + w), \quad (B2)$$

which is equivalent to the familiar form of isostatic balance:

$$\rho_m g (L + w) = \rho_L g L, \quad (B3)$$

where g is gravitational acceleration.

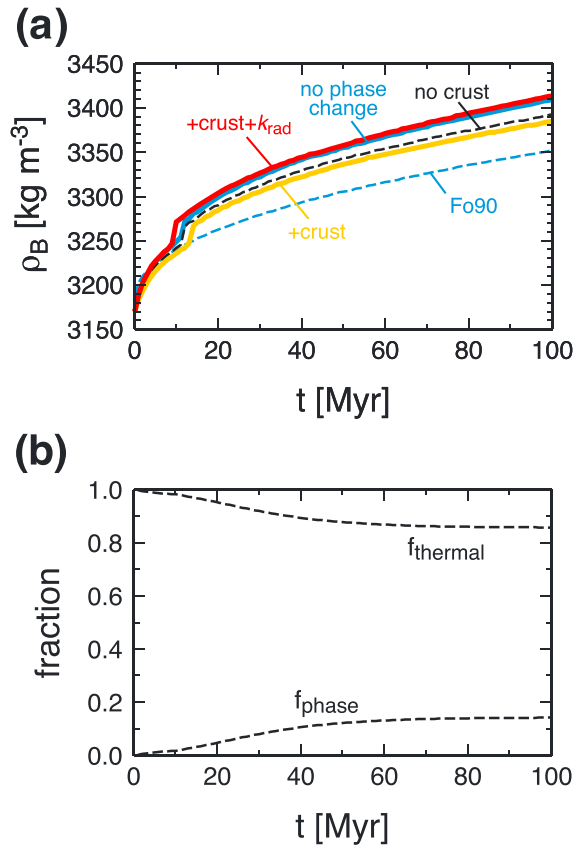


Figure B2. (a) Temporal variation of ρ_B in equation (B5). Line legend is the same as in Figure 4. (b) Fractions of subsidence due to thermal contraction and phase transitions, based the two cases of + crust + k_{rad} and no phase change.

When the overlying medium is sea water, an extra amount of subsidence, Δw , is necessary to achieve an isostatic balance (Figure B1b),

$$\rho_B g \Delta w = \rho_w g (w + \Delta w), \quad (B4)$$

where ρ_B is the density at the depth of compensation (i.e., the minimum depth where $\rho(Z', t) = \rho(Z', 0)$ is achieved), and ρ_w is the density of sea water (1030 kg m⁻³). By combining equations (B1) and (B4), we have

$$w + \Delta w = \frac{\rho_B}{\rho_B - \rho_w} \int_0^\infty \left(1 - \frac{\rho(Z', 0)}{\rho(Z', t)} \right) dz'. \quad (B5)$$

The above equation is identical to the isostasy formula derived by *Grose and Afonso* [2013] except that instead of ρ_B , they use ρ_b , which is the average density of the initial mantle column (reported as ~ 3200 kg m⁻³ in *Grose and Afonso* [2013]). It should be clear from the above derivation, however, that ρ_B must be used. The temporal variation of ρ_B is shown in Figure B2a, and it can be seen that ρ_B is in general substantially higher than ρ_b , so the use of the correct isostasy formula, i.e., equation (B5), yields smaller seafloor subsidence.

Appendix C: Calculation of Surface Topography

The effect of radiogenic heat production on seafloor subsidence is quantified in a manner similar to the work of *Korenaga* [2015] with a few modifications as described below. First, because we are concerned only with the half-space cooling phase of lithospheric evolution, thermal evolution can be calculated analytically without considering the possibility of convective instability. We use the following analytical solution for instantaneous cooling with uniform heating [*Carslaw and Jaeger*, 1959]:

$$T^*(t^*, z^*) = \left(T_0^* + H^* t^* + \frac{1}{2} H^* z^{*2} \right) \operatorname{erf} \left(\frac{z^*}{2\sqrt{t^*}} \right) + H^* z^* \sqrt{\frac{t^*}{\pi}} \exp \left(-\frac{z^{*2}}{4t^*} \right) - \frac{1}{2} H^* z^{*2}, \quad (C1)$$

where asterisks denote nondimensionalization, T is temperature, t is time, z is depth, T_0 is initial temperature, and H is internal heat production. Because we use the Boussinesq approximation [Schubert *et al.*, 2001] to solve fluid flow, the above temperature corresponds to potential temperature (referenced at the surface), and T_0 is constant at all depths. Temperature is normalized by the temperature scale ΔT , which is the difference between the surface temperature and the present-day potential temperature of the average mantle (1350 K). Depth is normalized by the whole mantle depth (2890 km), and time is normalized by the diffusion time scale, D^2/κ , where κ is thermal diffusivity ($10^{-6} \text{ m}^2 \text{ s}^{-1}$). Heat production is normalized by $k\Delta T/(\rho_0 D^2)$, where k and ρ_0 are thermal conductivity and average mantle density (4400 kg m^{-3}), respectively. The exact value of k will be determined by dimensionalizing the predicted heat flow with the observed heat flow ($550/\sqrt{t}$, where t is age in Myr and heat flow is in mW m^{-2} [Korenaga and Korenaga, 2008]). The analytical solution of surface heat flow is

$$q^*(t^*) = \frac{T_0^*}{\sqrt{\pi t^*}} + 2H^* \sqrt{\frac{t^*}{\pi}}, \quad (\text{C2})$$

in which heat flow is scaled by $k\Delta T/D$. Once k is found, internal heat production can be dimensionalized [see Korenaga, 2015, equation (13)].

The use of the above thermal structure for the entire domain of the suboceanic mantle is obviously rather too simplistic. In the real mantle, slight thermal anomalies produced by radiogenic heating are expected to be disturbed to some extent by convective currents. Modeling the effect of such convective currents, however, is beyond the scope of this study and is also subject to large uncertainties, because it is still difficult to resolve present-day flow patterns in the deep mantle. What we are trying to quantify is the overall effect of radiogenic heating in the age-depth systematics of seafloor, and our modeling effort is adequate for this purpose.

Second, the initial temperature T_0^* is set to unity in Korenaga [2015], which corresponds to the limiting case of no secular cooling of the mantle. We explore the effect of secular cooling by increasing T_0^* with t^* accordingly to a chosen cooling rate. This would act to reduce the subsidence rate because older parts of the lithosphere would have cooled less efficiently as they formed above a hotter mantle. Strictly speaking, the amount of radiogenic heating also changes slightly because of radioactive decay, but such change is of negligible influence for the duration of 100 Myr.

As in Korenaga [2015], we use $T^*(t^*, z^*)$ to construct a two-dimensional thermal structure $T^*(x^*, z^*)$; the duration of 100 Myr is mapped to the horizontal extent of 6000 km, which is equivalent to assuming the plate velocity of 6 cm yr^{-1} . We then calculate instantaneous Stokes flow and use the vertical normal stress to calculate surface topography [e.g., Davies, 1988]. The effect of internal heating H^* on seafloor subsidence can be extracted by comparing with the reference case of $H^* = 0$. For Stokes flow calculation, Korenaga [2015] used purely temperature-dependent viscosity, but the third and last modification in this study is that we consider depth dependency as well (Figure 6a). For the temperature dependency of viscosity, we use the Frank-Kamenetskii parameter of 20, which is equivalent to the activation energy of $\sim 300 \text{ kJ mol}^{-1}$.

Whereas Stokes flow and thus surface topography are calculated with viscosity variations in both vertical and horizontal direction, using the finite element method, the topography kernels shown in Figure 6c are calculated using purely depth-dependent viscosity in which the effect of temperature-dependent viscosity is approximated by the high-viscosity lid (for the depth less than 100 km). The concept of topography kernel is valid only when viscosity variations are limited to the vertical direction [Parsons and Daly, 1983], and topographic kernels are calculated, using the propagator matrix method [Hager and O'Connell, 1981], solely for the purpose of interpretation in this study.

The surface topography calculated in the above is all thermal origin, so the reduction in subsidence rate caused by internal heating is only applicable to the thermal contraction part of the total subsidence (f_{thermal} in Figure B2). In Figure 6d, therefore, the effects of incomplete viscous relaxation and internal heating on subsidence rate, s , are taken into account as

$$s = s_0 f_{\text{phase}} + s_0 f_{\text{thermal}} (1 - r_c - r_H), \quad (\text{C3})$$

where s_0 is the total subsidence rate before any correction ($\sim 500 \text{ m Myr}^{-1/2}$), f_{phase} , and f_{thermal} are the fractions of subsidence due to solid phase transitions (0.16) and thermal contractions (0.84), respectively, and r_c and r_H denote relative reduction due to, respectively, thermal cracking (up to 0.2 [Korenaga, 2007a]) and internal heating (e.g., ~ 0.2 for 10 TW with the secular cooling of 100 K Gyr^{-1} , Figure 6b).

Acknowledgments

This material is based upon work supported by the U.S. National Aeronautics and Space Administration through the NASA Astrobiology Institute under Cooperative agreement NNA15BB03A issued through the Science Mission Directorate. This work is theoretical in nature, and no specific data sources were used outside of works cited. The authors thank J.C. Afonso and an anonymous reviewer for constructive comments.

References

- Afonso, J. C., G. Ranalli, and M. Fernandez (2007), Density structure and buoyancy of the oceanic lithosphere revisited, *Geophys. Res. Lett.*, *34*, L10302, doi:10.1029/2007GL029515.
- Afonso, J. C., M. Fernandez, G. Ranalli, W. L. Griffin, and J. A. D. Connolly (2008), Integrated geophysical-petrological modeling of the lithosphere and sublithospheric upper mantle: Methodology and applications, *Geochem. Geophys. Geosyst.*, *9*, Q05008, doi:10.1029/2007GC001834.
- Angel, R. J. (2004), Equations of state of plagioclase feldspars, *Contrib. Mineral. Petrol.*, *146*, 506–512.
- Asimow, P., and M. Ghiorso (1998), Algorithmic modifications extending MELTS to calculate subsolidus phase relations, *Am. Mineral.*, *83*, 1127–1132.
- Berman, R. G. (1988), Internally-consistent thermodynamic data for minerals in the system Na₂O-K₂O-CaO-MgO-FeO-Fe₂O₃-Al₂O₃-SiO₂-TiO₂-H₂O-CO₂, *J. Petrol.*, *29*, 455–522.
- Bouhifd, M. A., D. Andraut, G. Fiquet, and P. Richet (1996), Thermal expansion of forsterite up to the melting point, *Geophys. Res. Lett.*, *23*, 1143–1146.
- Buck, W. R., and E. M. Parmentier (1986), Convection beneath young oceanic lithosphere: Implications for thermal structure and gravity, *J. Geophys. Res.*, *91*, 1961–1974.
- Carlson, R. L., and H. P. Johnson (1994), On modeling the thermal evolution of the oceanic upper mantle: An assessment of the cooling model, *J. Geophys. Res.*, *99*, 3201–3214.
- Carlsaw, H. S., and J. C. Jaeger (1959), *Conduction of Heat in Solids*, 2nd ed., Oxford Univ. Press, New York.
- Davies, G. F. (1988), Role of the lithosphere in mantle convection, *J. Geophys. Res.*, *93*, 10,451–10,466.
- Davies, G. F. (1992), On the emergence of plate tectonics, *Geology*, *20*, 963–966.
- Davis, E. E., and C. R. B. Lister (1974), Fundamentals of ridge crest topography, *Earth Planet. Sci. Lett.*, *21*, 405–413.
- Dumoulin, C., M.-P. Doin, and L. Fleitout (2001), Numerical simulations of the cooling of an oceanic lithosphere above a convective mantle, *Phys. Earth Planet. Inter.*, *125*, 45–64.
- Fei, Y. (1995), Thermal expansion, in *A Handbook of Physical Constants*, pp. 29–44, AGU, Washington, D. C.
- Ghiorso, M., M. Hirschmann, P. Reiners, and V. Kress (2002), pMELTS: A revision of MELTS for improved calculation of phase relations and major element partitioning related to partial melting of the mantle to 3 GPa, *Geochem. Geophys. Geosyst.*, *3*, 1030, doi:10.1029/2001GC000217.
- Grose, C. J., and J. C. Afonso (2013), Comprehensive plate models for the thermal evolution of oceanic lithosphere, *Geochem. Geophys. Geosyst.*, *14*, 3751–3778, doi:10.1002/ggge.20232.
- Gurnis, M., C. Hall, and L. Lavie (2004), Evolving force balance during incipient subduction, *Geochem. Geophys. Geosyst.*, *5*, Q07001, doi:10.1029/2003GC000681.
- Haavik, C., S. Stølen, H. Fjellvåg, M. Hanfland, and D. Häusermann (2000), Equation of state of magnetite and its high-pressure modification: Thermodynamics of the Fe-O system at high pressure, *Am. Mineral.*, *85*, 514–523.
- Hager, B. H., and R. J. O'Connell (1981), A simple global model of plate dynamics and mantle convection, *J. Geophys. Res.*, *86*, 4843–4867.
- Hart, S. R., and A. Zindler (1986), In search of a bulk-earth composition, *Chem. Geol.*, *57*, 247–267.
- Hasterok, D. (2013), A heat flow based cooling model for tectonic plates, *Earth Planet. Sci. Lett.*, *361*, 34–43.
- Herzberg, C., and M. J. O'Hara (2002), Plume-associated ultramafic magmas of Phanerozoic age, *J. Petrol.*, *43*, 1857–1883.
- Herzberg, C., P. D. Asimow, N. Arndt, Y. Niu, C. M. Lesher, J. G. Fitton, M. J. Cheadle, and A. D. Saunders (2007), Temperatures in ambient mantle and plumes: Constraints from basalts, picrites, and komatiites, *Geochem. Geophys. Geosyst.*, *8*, Q02206, doi:10.1029/2006GC001390.
- Herzberg, C., K. Condie, and J. Korenaga (2010), Thermal evolution of the Earth and its petrological expression, *Earth Planet. Sci. Lett.*, *292*, 79–88.
- Hirth, G., and D. Kohlstedt (2003), Rheology of the upper mantle and the mantle wedge: A view from the experimentalists, in *Inside the Subduction Factory*, edited by J. Eiler, pp. 83–105, AGU, Washington, D. C.
- Hofmeister, A. M. (2005), Dependence of diffusive radiative transfer on grain-size, temperature, and Fe-content: Implications for mantle processes, *J. Geodyn.*, *40*, 51–72.
- Hofmeister, A. M. (2007), Pressure dependence of thermal transport properties, *Proc. Natl. Acad. Sci. U.S.A.*, *104*, 9192–9197.
- Holland, T. J. B., and R. Powell (1998), An internally consistent thermodynamic data set for phases of petrological interest, *J. Metamorphic Geol.*, *16*, 309–343.
- Huang, J., and S. Zhong (2005), Sublithospheric small-scale convection and its implications for residual topography at old ocean basins and the plate model, *J. Geophys. Res.*, *110*, B05404, doi:10.1029/2004JB003153.
- Hynes, A. (2005), Buoyancy of the oceanic lithosphere and subduction initiation, *Int. Geol. Rev.*, *47*, 938–951.
- International Heat Flow Commission of IASPEI (2011), *Global Heat Flow Database*. [Available <http://www.heatflow.und.edu/index2.html>, (last update: January 11, 2011).]
- Jochum, K. P., A. W. Hofmann, E. Ito, H. M. Seufert, and W. M. White (1983), K, U and Th in mid-ocean ridge basalt glasses and heat production, K/U and K/Rb in the mantle, *Nature*, *306*, 431–436.
- Kasting, J. F., and D. Catling (2003), Evolution of a habitable planet, *Annu. Rev. Astron. Astrophys.*, *41*, 429–463.
- Kinzler, R. J. (1997), Melting of mantle peridotite at pressures approaching the spinel to garnet transition: Application to mid-ocean ridge basalt petrogenesis, *J. Geophys. Res.*, *102*, 852–874.
- Kinzler, R. J., and T. L. Grove (1992), Primary magmas of mid-ocean ridge basalts: 2. Applications, *J. Geophys. Res.*, *97*, 6907–6926.
- Korenaga, J. (2007a), Effective thermal expansivity of Maxwellian oceanic lithosphere, *Earth Planet. Sci. Lett.*, *257*, 343–349.
- Korenaga, J. (2007b), Thermal cracking and the deep hydration of oceanic lithosphere: A key to the generation of plate tectonics?, *J. Geophys. Res.*, *112*, B05408, doi:10.1029/2006JB004502.
- Korenaga, J. (2008), Urey ratio and the structure and evolution of Earth's mantle, *Rev. Geophys.*, *46*, RG2007, doi:10.1029/2007RG000241.
- Korenaga, J. (2009), How does small-scale convection manifest in surface heat flux?, *Earth Planet. Sci. Lett.*, *287*, 329–332.
- Korenaga, J. (2013), Initiation and evolution of plate tectonics on Earth: Theories and observations, *Annu. Rev. Earth Planet. Sci.*, *41*, 117–151.
- Korenaga, J. (2015), Seafloor topography and the thermal budget of Earth, in *The Interdisciplinary Earth: A Volume in Honor of Don L. Anderson*, edited by G. R. Foulger, M. Lustrino, and S. D. King, pp. 167–185, GSA Spec. Paper 514 and AGU Spec. Publ. 71, Geol. Soc. of Am., Boulder, Colo.
- Korenaga, J., and T. H. Jordan (2002), On "steady-state" heat flow and the rheology of oceanic mantle, *Geophys. Res. Lett.*, *29*, 2056, doi:10.1029/2002GL016085.
- Korenaga, J., and S. Karato (2008), A new analysis of experimental data on olivine rheology, *J. Geophys. Res.*, *113*, B02403, doi:10.1029/2007JB005100.

- Korenaga, J., and P. B. Kelemen (2000), Major element heterogeneity of the mantle source in the North Atlantic igneous province, *Earth Planet. Sci. Lett.*, *184*, 251–268.
- Korenaga, T., and J. Korenaga (2008), Subsidence of normal oceanic lithosphere, apparent thermal expansivity, and seafloor flattening, *Earth Planet. Sci. Lett.*, *268*, 41–51.
- Kroll, H., A. Kirfel, R. Heinemann, and B. Barbier (2012), Volume thermal expansion and related thermophysical parameters in the Mg,Fe olivine solid-solution series, *Eur. J. Mineral.*, *24*, 935–956.
- Langmuir, C. H., E. M. Klein, and T. Plank (1992), Petrological systematics of mid-ocean ridge basalts: Constraints on melt generation beneath ocean ridges, in *Mantle Flow and Melt Generation at Mid-Ocean Ridges*, *Geophys. Monogr. Ser.*, vol. 71, edited by J. Phipps Morgan, D. K. Blackman, and J. M. Sinton, pp. 183–280, AGU, Washington, D. C.
- Lv, M., X. Liu, S. R. Shieh, T. Xie, F. Wang, C. Presher, and V. B. Prakapenka (2016), Equation of state of synthetic qandilite Mg_2TiO_4 at ambient temperature, *Phys. Chem. Minerals*, *43*, 301–306.
- Lyubetskaya, T., and J. Korenaga (2007), Chemical composition of Earth's primitive mantle and its variance: 1. Methods and results, *J. Geophys. Res.*, *112*, B03211, doi:10.1029/2005JB004223.
- McKenzie, D., and M. J. Bickle (1988), The volume and composition of melt generated by extension of the lithosphere, *J. Petrol.*, *29*, 625–679.
- McKenzie, D. P. (1967), Some remarks on heat flow and gravity anomalies, *J. Geophys. Res.*, *72*, 6261–6273.
- Mitrovica, J. X., and A. M. Forte (2004), A new inference of mantle viscosity based upon joint inversion of convection and glacial isostatic adjustment data, *Earth Planet. Sci. Lett.*, *225*, 177–189.
- Mullet, B. G., J. Korenaga, and S.-I. Karato (2015), Markov chain Monte Carlo inversion for the rheology of olivine single crystals, *J. Geophys. Res. Solid Earth*, *120*, 3142–3172, doi:10.1002/2014JB011845.
- Nestola, F., B. Perotto, G. B. Andreozzi, E. Bruschini, and F. Bosi (2014), Pressure-volume equation of state for chromite and magnesiochromite: A single-crystal X-ray diffraction investigation, *Am. Mineral.*, *99*, 1248–1253.
- O'Neill, H. S. C., S. A. T. Redfern, S. Kesson, and S. Short (2003), An in situ neutron diffraction study of cation disordering in synthetic qandilite Mg_2TiO_4 at high temperatures, *Am. Mineral.*, *88*, 860–865.
- Oxburgh, E. R., and E. M. Parmentier (1977), Compositional and density stratification in oceanic lithosphere—Causes and consequences, *J. Geol. Soc. London*, *133*, 343–355.
- Palme, H., and H. S. C. O'Neill (2003), Cosmochemical estimates of mantle composition, in *Treatise on Geochemistry*, vol. 2, edited by H. D. Holland and K. K. Turekian, pp. 1–38, Elsevier, Netherlands.
- Parsons, B. (1982), Causes and consequences of the relation between area and age of the ocean floor, *J. Geophys. Res.*, *87*, 289–302.
- Parsons, B., and S. Daly (1983), The relationship between surface topography, gravity anomalies, and temperature structure of convection, *J. Geophys. Res.*, *88*, 1129–1144.
- Parsons, B., and J. G. Sclater (1977), An analysis of the variation of ocean floor bathymetry and heat flow with age, *J. Geophys. Res.*, *82*, 803–827.
- Pond, S., and G. L. Pickard (1983), *Introductory Dynamical Oceanography*, 2nd ed., Pergamon, Boston.
- Ringwood, A. E., and D. H. Green (1964), Experimental investigations bearing on the nature of the Mohorovicic discontinuity, *Nature*, *201*, 566–567.
- Schubert, G., D. L. Turcotte, and P. Olson (2001), *Mantle Convection in the Earth and Planets*, Cambridge Univ. Press, New York.
- Schutt, D. L., and C. E. Leshner (2006), Effects of melt depletion on the density and seismic velocity of garnet and spinel ilmenite, *J. Geophys. Res.*, *111*, B05401, doi:10.1029/2003JB002950.
- Smith, P. M., and P. D. Asimow (2005), Adibat_1ph: A new public front-end to the MELTS, pMELTS, and pHMELTS models, *Geochem. Geophys. Geosyst.*, *6*, Q02004, doi:10.1029/2004GC000816.
- Smyth, J. R., and T. C. McCormick (1995), Crystallographic data for minerals, in *A Handbook of Physical Constants*, pp. 1–17, AGU, Washington, D. C.
- Stein, C. A., and S. Stein (1992), A model for the global variation in oceanic depth and heat flow with lithospheric age, *Nature*, *359*, 123–129.
- Stixrude, L., and C. Lithgow-Bertelloni (2005), Thermodynamics of mantle minerals. I. Physical properties, *Geophys. J. Int.*, *162*, 610–632.
- Stixrude, L., and C. Lithgow-Bertelloni (2011), Thermodynamics of mantle minerals. II. Phase equilibria, *Geophys. J. Int.*, *184*, 1180–1213.
- Sun, S. S., and W. F. McDonough (1989), Chemical and isotopic systematics of oceanic basalts: Implications for mantle composition and processes, in *Magmatism in the Ocean Basins*, edited by A. D. Saunders and M. J. Norry, pp. 313–345, London.
- Tribaudino, M., R. J. Angel, F. Camara, F. Nestola, D. Pasqual, and I. Margiolaki (2010), Thermal expansion of plagioclase feldspars, *Am. Mineral.*, *160*, 899–908.
- Tribaudino, M., M. Bruno, F. Nestola, D. Pasqual, and R. J. Angel (2011), Thermoelastic and thermodynamic properties of plagioclase feldspars from thermal expansion measurements, *Am. Mineral.*, *96*, 992–1002.
- Turcotte, D. L., and G. Schubert (1982), *Geodynamics: Applications of Continuum Physics to Geological Problems*, John Wiley, New York.
- Valencia, D., and R. J. O'Connell (2009), Convection scaling and subduction on Earth and super-Earths, *Earth Planet. Sci. Lett.*, *286*, 492–502.
- Valencia, D., D. D. Sasselov, and R. J. O'Connell (2007), Inevitability of plate tectonics on super-Earths, *Astrophys. J.*, *670*, 45–48.
- Zlotnik, S., J. C. Afonso, P. Diez, and M. Fernandez (2008), Small-scale gravitational instabilities under the oceans: Implications for the evolution of oceanic lithosphere and its expression in geophysical observables, *Philos. Mag.*, *88*, 1–11.